ADVANCED FUNCTIONAL MATERIALS
www.afm-journal.de

A Self-Powered Angle Measurement Sensor Based on Triboelectric Nanogenerator

*Ying Wu, Qingshen Jing, Jun Chen, Peng Bai, Junjie Bai, Guang Zhu, Yuanjie Su, and Zhong Lin Wang**

A self-powered, sliding electrification based quasi-static triboelectric sensor (QS-TES) for detecting angle from rotating motion is reported. This innovative, cost-effective, simply-designed QS-TES has a two-dimensional planar structure, which consists of a rotator coated with four channel coded Cu foil material and a stator with a fluorinated ethylenepropylene film. On the basis of coupling effect between triboelectrification and electrostatic induction, the sensor generates electric output signals in response to mechanical rotating motion of an object mounted with the sensor. The sensor can read and remember the absolute angular position, angular velocity, and acceleration regardless being continuously monitored or segmented monitored. Under the rotation speed of 100 r min^{-1}, the output voltage of the sensor reaches as high as 60 V. Given a relatively low threshold voltage of ±0.5 V for data processing, the robustness of the device is guaranteed. The resolution of the sensor is 22.5° and can be further improved by increasing the number of channels. Triggered by the output voltage signal, the rotating characteristics of the steering wheel can be real-time monitored and mapped by being mounted to QS-TES. This work not only demonstrates a new principle in the field of angular measurement but also greatly expands the applicability of triboelectric nanogenerator as self-powered sensors.

1. Introduction

Angle measurement is a common and essential technology in industrial and manufacturing systems. Over the past decade, major advances have occurred in angle measurement based on optoelectrical transformation,[1,2] electrical effects,[3,4] and electromagnetic induction.[5,6] However, widespread usage of these techniques is likely to be shadowed by possible limitations, such as structure complexity, requirement of sophisticated materials, and reliance on external power source. Recently, triboelectric nanogenerator (TENG),[7–14] a creative invention based on the coupling of the universally known contact electrification effect and electrostatic induction, has been extensively explored to establish cost-effective and robust self-powered sensing systems, including vibration sensor,[15] motion sensor,[16] acoustic sensor,[17] biosensor,[18] displacement vector sensor,[19] acceleration sensor,[20] wind vector sensor,[21] tactile sensor,[22] tracking sensor,[23] chemical sensor,[24,25] and so on. Here, we, for the first time, introduce a new principle in angle measurement by fabricating a quasi-static triboelectric sensor (QS-TES). The as-fabricated self-powered sensor is based on a periodic contact/separation between foam with Cu material and a fluorinated ethylenepropylene (FEP) film. The absolute angular position of rotating object can be read and remembered regardless being continuously monitored with the self-powered sensor. Under the rotation speed of 100 r min^{-1}, the output voltage of the sensor reaches as high as 60 V. Comparing with the threshold voltage for the data processing which is ±0.5 V, the robustness of the device is guaranteed. The resolution of the sensor is 22.5° and can be further improved by increasing the number of channels. Triggered by the output voltage signal, the rotating characteristics of the steering wheel can be real-time monitored and mapped by being mounted to QS-TES. This work not only presents a new principle in the field of angle measurement but also greatly expands the applicability of TENGs as self-powered sensors.

Y. Wu, Q. Jing, J. Chen, P. Bai, G. Zhu, Y. Su,
Prof. Z. L. Wang
School of Materials Science and Engineering
Georgia Institute of Technology
Atlanta, GA 30332–0245, USA
E-mail: zlwang@gatech.edu
Y. Wu, J. Bai
School of Electrical and Information Engineering
Chongqing Univeristy of Science and Technology
Chongqing 401331, China
Prof. Z. L. Wang
Beijing Institute of Nanoenergy and Nanosystems
Chinese Academy of Sciences
Beijing 100083, China

DOI: 10.1002/adfm.201403828

2. Results and Discussion

The presented self-powered angle sensor has a multi-layered structure, which consists of two parts, a rotator and a stator, as sketched in **Figure 1**a. The rotator is composed of three layers: a rigid substrate layer made of acrylic, a soft supporting layer made of pattern-carved foam followed by a deposited layer of Cu forming foil sectors as an electrification layer (Figure 1b). The rotator is a collection of radially arrayed sectors separated

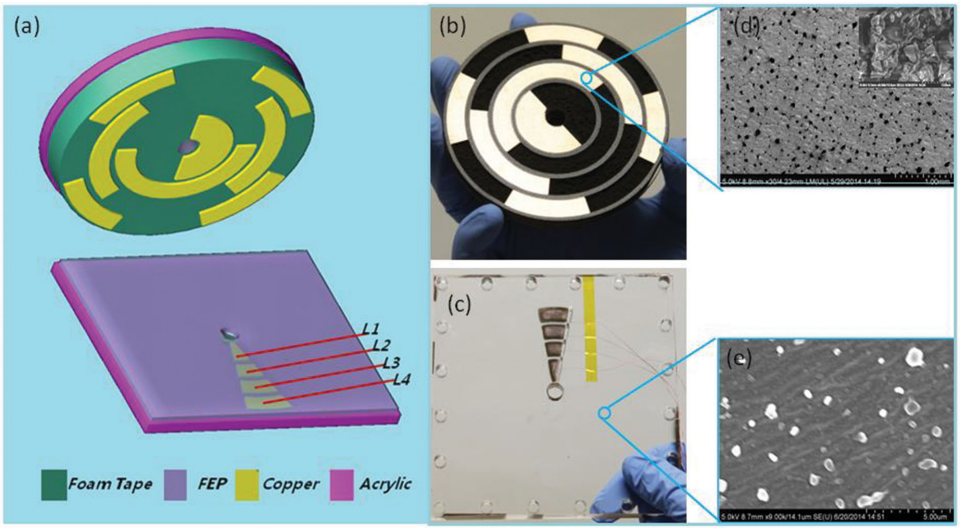

Figure 1. Structure design of self-powered angel monitor based on TENG. a) Schematic illustrations of the self-powered angel sensor, which has two parts, that is, a rotator and a stator. b) Photograph of a rotator. SEM picture d) reveals the Cu foil coated on the foam. The inset is the enlarged SEM image. c) Photograph of a stator, in which the through-holes along edges are for mounting purpose (scale bar, 2 cm). e) SEM image showing PTFE particles spread on the surface of FEP.

by equal-degree intervals in between. A layer of Cu thin film was deposited on the foam to form a coded Cu foil sector. A Scanning Electron Microscope (SEM) image of the Cu film is shown in Figure 1d, in which the inset is the SEM image at a higher magnification. The stator has a vertical-stacked structure consisting of three layers (Figure 1c). First, a layer of Cu was deposited onto the acrylic substrate, and then, a layer of FEP was spread out on the Cu surface, working as an electrification layer. Here, FEP and copper were selected as the contact materials for generating triboelectric charges due to their large difference in electron affinity. As demonstrated in an SEM image in Figure 1e, spherical polytetrafluoroethylene (PTFE) nanoparticles were utilized as lubricant to reduce friction and to further improve energy conversion efficiency. To operate, the stator of the sensor will be anchored while the rotator rotates relatively for an angle measurement. When the monitored object rotates, the rotator sliding along the FEP film, where alternating flows of electrons are induced between the Cu bottom electrodes and the ground. The output voltage reflects the code of Cu foil sectors on the rotator, which corresponds to the angle difference. The angel can be obtained by calculated from the output voltage signal.

The operation of the TENG sensor relies on relative rotation between the rotator and the stator, in which a unique coupling between triboelectrification and electrostatic induction gives rise to alternating flow of electrons between electrodes. The electricity-generating process is elaborated through a basic unit in **Figure 2**. We define the initial state (Figure 2a-I) and the final state (Figure 2a-III) as the states when the rotator is aligned with bottom electrode and completely off aligned the bottom electrode, respectively. The intermediate state (Figure 2a-II) represents the transitional process in which the rotator spins from the initial position to the final position. Since the rotator and the stator are in direct contact, triboelectrification creates charge transfer on contacting surfaces, with negative charges generated on the FEP and positive ones on the metal[26,27] as illustrated in the cross-sectional view defined by an arbitrary intersection in Figure 2. Due to the law of charge conservation, the density of positive charges on the rotator is twice as much as that of negative ones on the stator because of unequal contact surface area of the two objects.

As shown in Figure 1, Cu is patterned on the disk to form the radially arrayed metal and nonmetal sectors, which result in the disk-shaped components with four channel circle. At the original position depicted in Figure 2a-I, due to the large difference in triboelectric polarity, FEP attracts electrons from the patterned electrode on the foam, leaving net negative charges on the FEP surface and an equal amount of positive charges on the foam. The generated negative triboelectric charges distribute evenly on the FEP film and remain for an extended period of time. These negative triboelectric charges on the FEP film induce positive charges on the Cu bottom electrode from the ground as induced charges. Once the Cu metal sector approaches the Cu bottom electrode, the positive triboelectric charges on the metal sectors will drive electrons to flow from the ground to the Cu electrode, screening the electric field from the charged electrodes. When the metal sector is aligned with the electrode, the negative charges were maximized on the Cu electrode, as sketched in Figure 2a-I. As the rotator Cu foil sector starts to move away from the Cu bottom electrode, the induced electrons will flow back to the ground, leaving fewer negative charges on the Cu electrode, as shown in Figure 2a-II. When the rotator come to its final state in Figure 2a-III as the Cu foil sector is just separated from the bottom electrode, leaving fewer positive charges on the Cu electrode.

In the open-circuit condition, electrons cannot transfer between electrodes. And, the open-circuit voltage is then defined as the electric potential difference between the electrode and ground, namely, $V_{oc} = U_e$.

The initial state corresponds to the minimum V_{oc}. Such a voltage then increases as the rotator starts to spin. Once the Cu foil sector on the rotator arrives at the area of the bottom

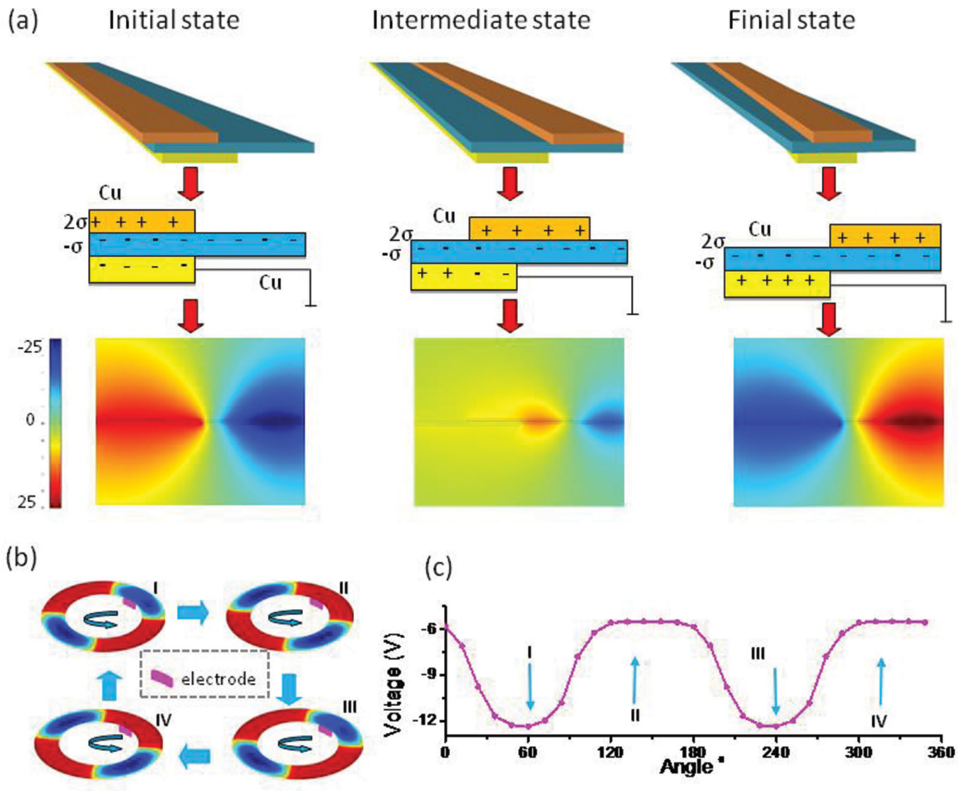

Figure 2. Schematics of operating principle of sensor. a) Electrical signal generating process. The three sections from top to bottom illustrate the three-dimensional schematic, charge distribution in open-circuit condition, and FEM simulation of charge density in short-circuit condition, respectively. (I) Initial state in which the rotator is aligned with the bottom electrode fully; (II) Intermediate state in which the rotator is spinning away from the initial position at an angle; (III) Final state in which the rotator is away from the bottom electrode fully. b) Working mechanism of one channel in one counter clockwise rotating cycle. c) Finite-element simulation of the output voltage of one channel corresponding to the state change shown in (b).

electrode, V_{oc} with the opposite polarity starts to build up and get the maximum value until the metal sector aligned with the bottom electrode completely. After that, the output voltage decreases with further rotation until reaches the final state. And a continuous rotation beyond the final state changes in a reversed way because of the periodic structure. The continuous variation of the V_{oc} is visualized via COMSOL in Movie 1, Supporting Information. On the basis of the assumption that the thickness of the dielectric layer is far smaller than its width dimension in Figure 2, an analytical model can be established, in which any overlapped region between the rotator and the electrode can be treated as a capacitor without consideration of the edge effect.[28,29] Then the V_{oc} can be analytically expressed by the following equations using Gauss theorem.[8]

$$\text{Initial state}: V_{OC} = \frac{d\sigma}{\varepsilon_0 \varepsilon_r} \quad (1)$$

$$\text{Final state}: V_{OC} = -\frac{d\sigma}{\varepsilon_0 \varepsilon_r} \quad (2)$$

where d is the thickness of the FEP layer, ε_0 is the dielectric constant of vacuum, ε_r is the relative dielectric constant of FEP. Equations (1) and (2) can only be used to illustrate the changing trend of the V_{oc} from negative peak to positive peak.

To derive a more quantitative understanding of the proposed signal-generating process of the QS-TES, the electric potential distribution and charge transfer process for the device are investigated through numerical calculation using COMSOL. Figure 2b illustrates the one channel electric potential distribution of the rotator when the rotator counter clockwise rotates one cycle. There are two metal sectors on the channel. The calculated electric potential as a function of the rotate angle is plotted in Figure 2c, exhibiting the simulation results of the open-circuit voltage in the QS-TES when rotator with metal sectors slide with and away from the bottom electrode. When the Cu foil sector on the rotator is fully aligned with the bottom electrode, the electric potential on the FEP film reaches a maximum as shown in Figure 2b-II,b-IV. The open-circuit voltage reaches the positive maximum as shown in Figure 2c. The open-circuit voltage is found to decrease dramatically as the distance between the rotator Cu foil sector and the bottom electrode gets larger. When the carved sector on the rotator fully aligns with the bottom electrode, the electric potential on the FEP film reaches a minimum as shown in Figure 2b-I,b-III. The open-circuit voltage reaches the negative maximum as shown in Figure 2c.

An array of Cu foil sectors can be applied along the multiple channels of foam with a certain interval in between. Consequently, as the rotator passes through the stator, an alternating flow of electrons occurs between the bottom electrode and the

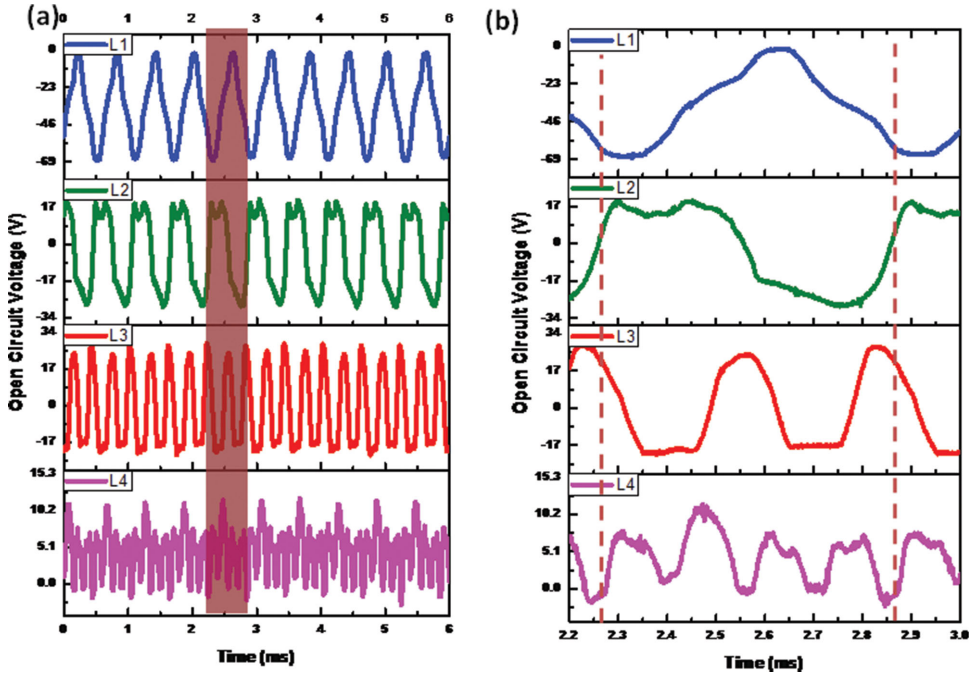

Figure 3. Results of electric measurements. a) Open-circuit voltage (V_{oc}) of four channels at a rotation rate of 100 r min^{-1}. b) Enlarged view of a cycle highlighted in (a).

ground, which generates the output signal with variation of high and low electrical level. Combining the Cu foil sector position with the output signal from the multiple channels, the coded information of the sensor indicating the motion angle of a rotating object can be revived. The whole processes composite the working principles of the QS-TES angle sensor. According to the working principles of angle measurement, the resolution of the sensor is $1/2^n$ which depending on the channel number n.

To characterize the performance of the QS-TES for angle measurement, the electric output from four electrodes was simultaneously measured. To control the rotation rate for quantitative measurement, a programmable rotary motor was connected to the rotator that was in coaxial alignment with the stator. The open-circuit voltage of four channels can be obtained at the same time. Shown in **Figure 3**a, the open-circuit voltage of four channels exhibits peaks in alternating contact between Cu foil sector and bottom electrodes. An enlarged view in Figure 3b displays an entire cycle of the voltage and corresponding positions of the rotator. Cu foil sector sliding toward the bottom electrode produces an increasing voltage peak, while departing causes a negative one, as illustrated in Figure 3b. The interval between neighbouring negative peak and positive peak of 1st channel (L_1) corresponds to one rotating cycle of the rotator. The negative peaks and positive peaks of 2nd channel (L_2), 3rd channel (L_3), and 4th channel (L_4) will display 1, 2, and 4 times, respectively, in one rotating cycle, which is responding to the Cu foil sector patterned on the foam. The open-circuit voltage, as shown in Figure 3, switches between zero and the maximum value of 60 V as the rotator repeatedly passes through the electrode. The experimental results are fully consistent with the above theoretical analysis and numerical simulations. The open-circuit voltages of four channels are shown in **Figure 4**, in which Figure 4b shows the enlarged view of the dashed box in Figure 4a. Each output signal from the 4 channels corresponding a location of the rotator. On one hand, when the output-circuit voltage of each channel reaches positive maximum, indicating that the Cu foil sector aligned with the bottom electrode. On the other hand, when the open-circuit voltage of each channel reaches negative maximum, indicating the carved sector aligned with the bottom electrode. Combining all the output voltage signal of four channels, the position of rotator can be localized and the motion angle of rotator can be calculated.

To demonstrate applications of the QS-TES for self-powered angle measurement, we mounted the sensor with the steering wheel together for monitoring and mapping the angle of the steering wheel in real time (Movie 2, Supporting Information). **Figure 5**a shows the self-powered angle measurement system. An external light emitting diode (LED) is connected between each channel electrode and the ground. When the steering wheel rotated, the external LED can be lighten as shown in Figure 5a-II–a-V. As shown in Figure 5b, the output voltages from the four channels were recorded and immediately displayed by indicators on a computer monitor when the steering wheel counter clockwise rotates for one cycle. The output signal can be considered as high electrical level ("1") when the open-circuit voltage is larger than the average voltage of each channel, and as low electrical level ("0") when the open-circuit voltage is smaller than the average voltage of each channel, respectively. The steering wheel rotates from the original position that corresponding to the carved sector, the output voltage of each channel is near to zero, which corresponds to the code "0000" and shown in Figure 5b-I. When the steering wheel rotates counter clockwise to the nine clock direction, the corresponding

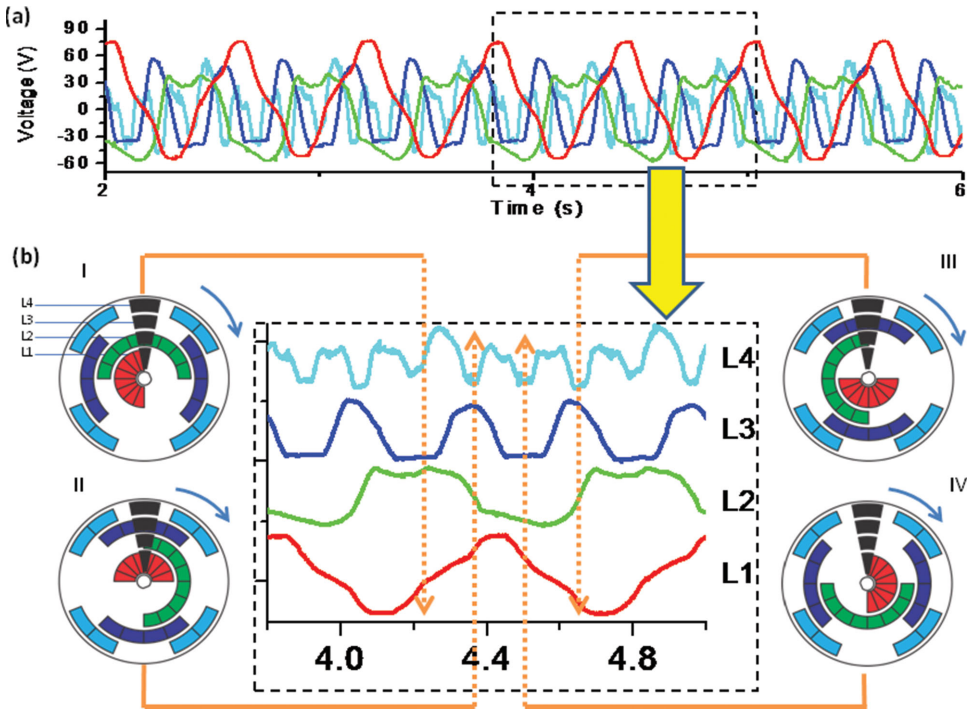

Figure 4. a) Measurement results of output voltage from four channels (L_1, L_2, L_3, L_4). b) Enlarged dash box area in a) describing the processing results of output voltage from four channels (L_1, L_2, L_3, L_4). The output voltages indicate the location of the rotator, corresponding to the decoded Cu foil sector of the sensor.

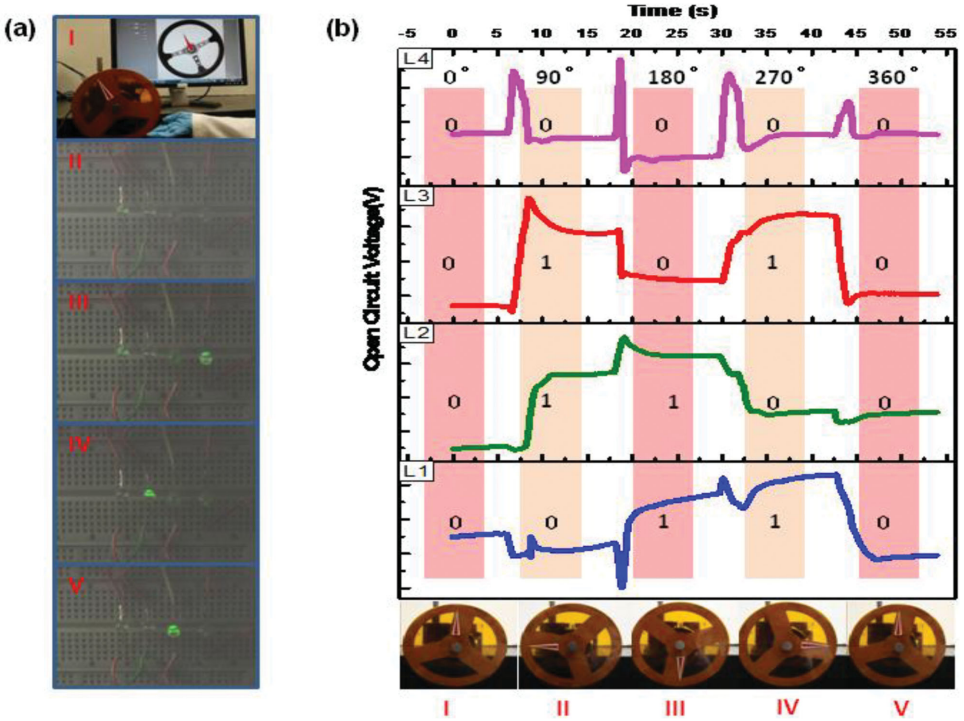

Figure 5. Self-powered QS-TES-based angle monitoring system of steering wheel. a) Optical image of the fabricated QS-TES angle monitoring system and the LED lighten by the self-powered angle monitoring system. b) Measured output voltage and real-time location mapping when the steering wheel counter clockwise rotates to the (I) 0°, (II) 90°, (III) 180°, (IV) 270°, and (V) 360°, the corresponding codes of output signal are "0000," "0110," "1100," "1010," and "0000," respectively.

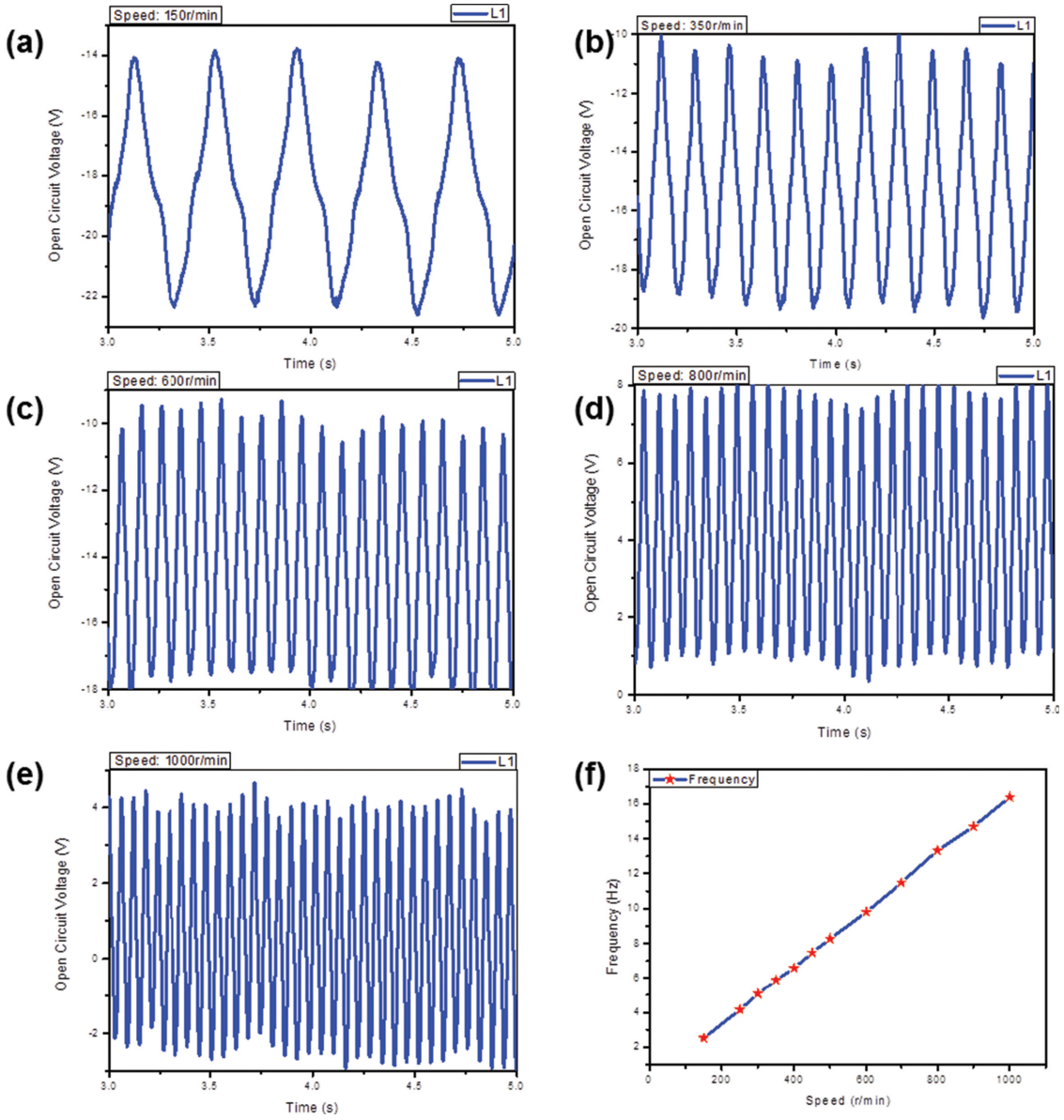

Figure 6. Demonstration of the QS-TES acting as a self-powered sensor for speed measurement. a) Open-circuit voltage of one channel at speed of 150 r min^{-1}. b) Open-circuit voltage of one channel at the speed of 350 r min^{-1}. c) Open-circuit voltage of one channel at the speed of 600 r min^{-1}. d) Open-circuit voltage of one channel at the speed of 800 r min^{-1}. e) Open-circuit voltage of one channel at the speed of 1000 r min^{-1}. f) Relationship between frequency and the speed. The rotating speed will influence the frequency of output voltage signal.

alternating voltages of four channels were measured at the same time, which indicates a value of the 90° and code "0110." The processing signal triggered the rotating of the steering wheel model, indicating the rotating angle of the steering wheel on the monitor. Figure 5b-II–b-V shows the voltage signals and the digital mapping results when the steering wheel rotates to the six, three, and twelve clock directions, which corresponding to the 180°, 270°, and 360°, respectively, and codes "1100," "1010," and "0000," respectively. Therefore, the positional information of the steering wheel can be immediately exhibited and directly perceived from the coded information.

Furthermore, the as-fabricated QS-TES can also be harnessed for angular speed measurement. Given a relationship between the voltage output and the rotating speed of QS-TES, the rotating speed can be calculated from the output voltage signal of one channel. Different rotating speed will lead to different periodical signal, thus, different frequency of the output voltage signal as shown in Equation (3):

$$\omega = 2\pi f \tag{3}$$

Figure 6 demonstrates the QS-TES acting as a self-powered sensor for rotating speed measurement. The open-circuit voltages at different rotating speed are shown in Figure 6a–e. Experimental results show that the frequency of the open-circuit voltage is monotonically increasing function of the rotating speed as shown in Figure 6f.

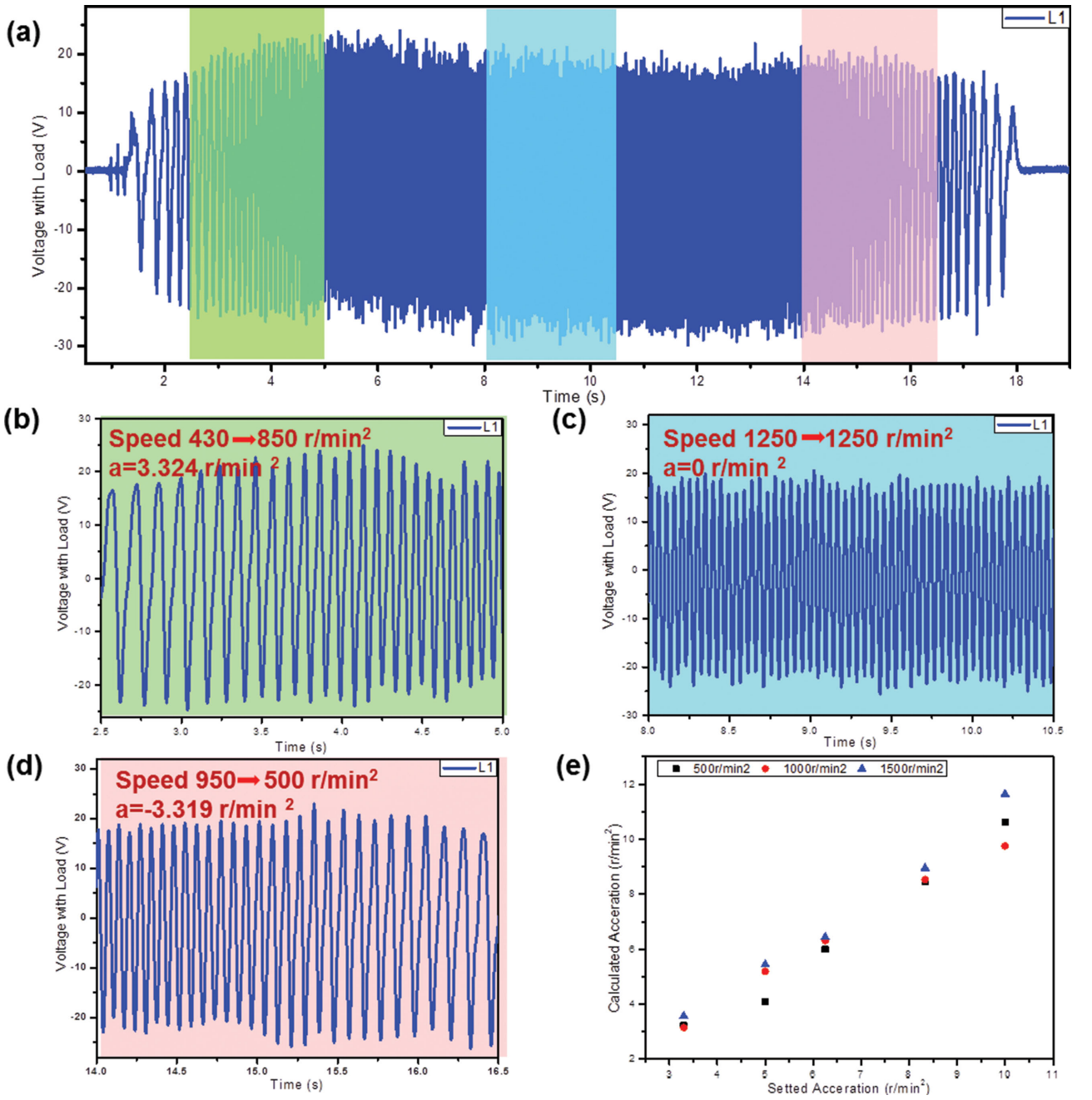

Figure 7. Demonstration of the QS-TES acting as a self-powered sensor for acceleration measurement. a) Output voltage with load of one channel when the speed increases from 0 r min^{-1} to 1250 r min^{-1} with acceleration of 3.33 r min^{-2} and speed decreases from 1250 r min^{-1} to 0 r min^{-1} with acceleration of –3.33 r min^{-2}. And enlarged views of the cycles were shown in b–d), corresponding to the three speed change phrases of the rotator, which is acceleration phrase (b), constant speed phrase (c), and deceleration phrase (d). f) Relationship between set acceleration and calculated acceleration at different rotating speed.

Additionally, the as-fabricated QS-TES can be harnessed for angular acceleration measurement. Assuming the angle difference of neighbouring sectors is $\theta = 2\pi/N$, if the time are ΔT_{n-1} and ΔT_n for the rotator rotating from $(n-1)$th sector to nth sector and from $(n-1)$th sector to nth sector, respectively, then the angle speeds are $\omega_{n-1} = \theta/\Delta T_{n-1}$ and $\omega_n = \theta/\Delta T_n$ for ΔT_{n-1} and ΔT_n, respectively. Angular acceleration for one period from ΔT_{n-1} to ΔT_n can be expressed as

$$\gamma_n = \frac{2(\omega_n - \omega_{n-1})}{(\Delta T_{n-1} + \Delta T_n)} = \frac{2\theta(\Delta T_n - \Delta T_{n-1})}{\Delta T_{n-1}\Delta T_n(\Delta T_{n-1} + \Delta T_n)} \quad (4)$$

Where the ΔT_n can be acquired with the counter. The detailed deduction of Equation (4) can be found in the Supporting Information.

Figure 7 demonstrates the QS-TES acting as a self-powered sensor for acceleration measurement. Increasing the rotating

speed of the QS-TES with fixed acceleration to one speed and decreasing the speed to zero with the same acceleration, the output voltage with load of one channel at different speed can be measured continuously as shown in Figure 7a. And enlarged views of the cycles were shown in Figure 7b–d, corresponding to the three speed change phrases of the rotator, which are acceleration phrase, constant speed phrase, and deceleration phrase. According to Equations (3) and (4), the speed and acceleration of the corresponding phrase can be calculated. The rotating speed of the rotator can be set as 500 r min^{-1}, 1000 r min^{-1}, 1500 r min^{-1}, respectively, and the acceleration can be set as 3.33 r min^{-2}, 5 r min^{-2}, 6.25 r min^{-2}, 8.33 r min^{-2}, and 10 r min^{-2} by changing the delay time of motor mounted with the QS-TES. The curves indicating the relationship between the calculated acceleration and set acceleration can be acquired based on the measured output voltage, which is shown in Figure 7e. The QS-TES acting as a self-powered sensor for monitoring the changed output voltage of one channel at different speed and different acceleration can be found in Figure S1, Supporting Information.

3. Conclusion

In summary, we first demonstrated a self-powered sensor for angle measurement using triboelectrification. The sliding of a rotator along a stator leads to charge transfer between the Cu bottom electrode and the ground, generating AC current peaks in the external circuit. By converting the mechanical rotation into electrical output signal, the sensor delivers an open-circuit voltage up to 60 V. An axial array of Cu foil sectors of rotator enables the detection of angle. And the angel can be monitored in real time by simultaneously reading the output voltage from different channels. Increasing the number of channels could refine the resolution for angle measurement. At the same time, the sensor can be used as self-powered angular speed and angular acceleration sensor. This work not only presents a new principle in the field of angle measurement but also greatly expands the applicability of TENGs as power self-powered sensors.

4. Experimental Section

Finite Element Analysis Method: The proposed simulation was based on electrostatic modeling software "Comsol Multiphysics 4.2." The quantity of the triboelectric charges on the surfaces of the stator and FEP film was assigned to be 20 μC m^{-2} as an equivalent result of friction. Open-circuit voltage was calculated at different rotating angles and channel 3 was chosen to be presented in Figure 2c. Width of electrodes and thickness of FEP was assigned with actual value. Relative permittivity of FEP was set as 2.0.

Fabrication of a QS-TES: The QS-TES consists of a stator and rotator. Stator: (1) Cut a disc-shaped polyimide substrate (25 mm) with lead wire hole as a substrate using a laser cutter; (2) Use photolithography (negative photoresist) to create exposed windows that define electrodes on the substrate; (3) Deposit metal layer by e-beam evaporation, followed by lift-off process to generate the electrode pattern on the substrate; (4) Connect four lead wires respectively to the electrodes; (5) a 0.5 g sample of commercial PTFE dispersion in which the PTFE nanoparticles were dissolved in isopropyl alcohol was sprayed on the surface of FEP thin films and dried in air. Adhere the thin layer of FEP (25 mm) on top of the electrode as an electrification layer. (6) Metal wires were connected to electrode located under the FEP film via lead wire hole from the bottom of the polyimide substrate, as outer electrode. Rotator: (1) Cut a disc-shaped polyimide substrate (25 mm) as a substrate with through-patterns that consist of radial arrayed sectors using a laser cutter; (2) Drill a through-hole that has a D-profile at the center of the rotator; (3) Use Ar/O_2 plasma (100 W) to do surface treatment on the substrate for 1 min; (4) Deposit a layer of Ti (10 nm) and then a layer of Cu (200 nm) on the rotator in sequence using a DC sputterer.

Experimental Setup for Electric Measurement: (1) Mount a rotary motor in an inverted way on a three-dimensional linear positioner; (2) Insert the D-profile shaft of the motor into the central hole of the rotator; (3) Align the rotator and the stator to make them in coaxial alignment by using the linear positioner; (4) Adjust height of the linear positioner so that the rotator and the stator are in contact. The output performance of the TENG was measured using a Stanford Research Systems apparatus. SR560 low-noise voltage amplifiers were used to record voltages.

Supporting Information

Supporting Information is available from the Wiley Online Library or from the author.

Acknowledgements

Y.W. and Q.J. contributed equally to this work. This work was supported by U.S. Department of Energy, Office of Basic Energy Sciences (DE-FG02–07ER46394), and the Thousands Talents program for pioneer researcher and his innovation team, China. Y.W. acknowledges the support of National Science Foundation of China via Grant No. 51105398. Y.W. would also like to acknowledge the fellowship from the China Scholarship Council (CSC).

Received: October 30, 2014
Revised: December 18, 2014
Published online: February 23, 2015

[1] R. D. Evans, N. M. Jokerst, R. B. Fair, *IEEE Sens. J.* **2008**, *5*, 628.
[2] C. Ciminelli, F. Dell'Olio, C. E. Campanella, M. N. Armenise, *Adv. Opt. Photonics* **2010**, *2*, 370.
[3] X. Zhang, L. Kang, W. Diao, *Int. Conf. Vehicular Electronics Safety, Xi'an, China*, IEEE, **2005**, 20.
[4] F. Vittorio, G. Alessio, M. Daniele, T. Andrea, *IEEE Instrum. Meas. Mag.* **2006**, *55*, 607.
[5] Z. Zhanga, F. Nia, Y. Dongb, M. Jina, H. Liua, *Sens. Actuators, A* **2013**, *194*, 196.
[6] H. V. Hoang, J. W. Jeon, *IEEE Ind. Electron.* **2011**, *58*, 3634.
[7] G. Zhu, J. Chen, Y. Liu, P. Bai, Y. Zhou, Q. Jing, C. Pan, Z. L. Wang, *Nano Lett.* **2013**, *13*, 2282.
[8] G. Zhu, J. Chen, T. Zhang, Q. Jingand, Z. L. Wang, *Nat. Commun.* **2014**, *5*, 3426.
[9] J. Yang, J. Chen, Y. Yang, H. Zhang, W. Yang, P. Bai, Y. Su, Z. L. Wang, *Adv. Eng. Mater.* **2014**, *4*, 1301322.
[10] G. Zhu, P. Bai, J. Chen, Z. L. Wang, *Nano Energy* **2013**, *2*, 688.
[11] Q. Jing, G. Zhu, P. Bai, Y. Xie, J. Chen, R. P. S. Han, Z. L. Wang, *ACS Nano* **2014**, *8*, 3836.
[12] W. Yang, J. Chen, G. Zhu, X. Wen, P. Bai, Y. Su, Y. Lin, Z. L. Wang, *Nano Res.* **2013**, *6*, 880.
[13] W. Yang, J. Chen, G. Zhu, J. Yang, P. Bai, Y. Su, Q. Jing, Z. L. Wang, *ACS Nano* **2013**, *7*, 11317.

[14] W. Yang, J. Chen, Q. Jing, J. Yang, X. Wen, Y. Su, G. Zhu, P. Bai, Z. L. Wang, *Adv. Funct. Mater.* **2014**, *24*, 4090.
[15] J. Chen, G. Zhu, W. Yang, Q. Jing, P. Bai, Y. Yang, T. C. Hou, Z. L. Wang, *Adv. Mater.* **2013**, *25*, 6094.
[16] W. Yang, J. Chen, X. Wen, Q. Jing, J. Yang, Y. Su, G. Zhu, W. Wu, Z. L. Wang, *ACS Appl. Mater. Interfaces* **2014**, *6*, 7479.
[17] J. Yang, J. Chen, Y. Liu, W. Yang, Y. Su, Z. L. Wang, *ACS Nano* **2014**, *8*, 2649.
[18] Y. Yang, H. Zhang, J. Chen, S. Lee, T. C. Hou, Z. L. Wang, *Energy Environ. Sci.* **2013**, *6*, 1744.
[19] Y. Yang, H. Zhang, J. Chen, Q. Jing, Y. S. Zhou, X. Wen, Z. L. Wang, *ACS Nano* **2013**, *7*, 7342.
[20] H. Zhang, Y. Yang, Y. Su, J. Chen, K. Adams, S. Lee, C. Hu, Z. L. Wang, *Adv. Funct. Mater.* **2014**, *24*, 1401.
[21] Y. Yang, G. Zhu, H. Zhang, J. Chen, X. Zhong, Z. H. Lin, Y. Su, P. Bai, X. Wen, Z. L. Wang, *ACS Nano* **2013**, *7*, 9461.
[22] Y. Yang, H. Zhang, Z. H. Lin, Y. S. Zhou, Q. Jing, Y. Su, J. Yang, J. Chen, C. Hu, Z. L. Wang, *ACS Nano* **2013**, *7*, 9213.
[23] Y. Su, G. Zhu, W. Yang, J. Yang, J. Chen, Q. Jing, Z. Wu, Y. Jiang, Z. L. Wang, *ACS Nano* **2014**, *8*, 3843.
[24] Z. H. Lin, G. Zhu, Y. S. Zhou, Y. Yang, P. Bai, J. Chen, Z. L. Wang, *Angew. Chem. Int. Ed.* **2013**, *52*, 1.
[25] H. Zhang, Y. Yang, Y. Su, J. Chen, C. Hu, Z. Wu, Y. Liu, C. P. Wong, Y. Bando, Z. L. Wang, *Nano Energy* **2013**, *2*, 693.
[26] G. Zhu, Y. S. Zhou, P. Bai, X. Meng, Q. Jing, J. Chen, Z. L. Wang, *Adv. Mater.* **2014**, *26*, 3788.
[27] F. Fan, Z. Tian, Z. L. Wang, *Nano Energy* **2012**, *1*, 328.
[28] G. Zhu, C. Pan, W. Guo, C. Chen, Y. Zhou, R. Yu, Z. L. Wang, *Nano Lett.* **2012**, *12*, 4960.
[29] S. Niu, Y. Liu, S. Wang, L. Lin, Y. Zhou, Y. Hu, Z. L. Wang, *Adv. Mater.* **2013**, *43*, 6184.